# Novel erbium(III) fluorinated β-diketonate complexes with *N,N*-donors for optoelectronics: from synthesis to solution-processed devices†

Pablo Martín-Ramos,[a] Manuela Ramos Silva,*[b] Carmen Coya,[c] Carlos Zaldo,[d] Ángel Luis Álvarez,[c] Susana Álvarez-García,[d] Ana M. Matos Beja[b] and Jesús Martín-Gil[e]

Three novel ternary $Er^{3+}$ complexes emitting in the C band transmission window for fiber optic communications have been synthesised and their structures have been elucidated by single crystal X-ray diffraction. The fluorinated β-diketonate ligand, 1,1,1-trifluoro-5,5-dimethyl-2,4-hexanedione, combines a good absorption cross-section in the ultraviolet region with reduction of non-radiative quenching of the $Er^{3+}$ emission, while the rigidity and bulkiness of the three different *N,N*-donors (2,2′-bipyridine, bathophenanthroline and 5-nitro-1,10-phenanthroline) have a pronounced impact on the emission intensity of luminescence. Furthermore, the choice of the ancillary ligand also determines the efficiency of the antenna effect, leading to complete quenching of the ligand-associated visible emission for the optimized complex with 5-nitro-1,10-phenanthroline. Solution processed 1.54 μm organic light-emitting diodes have been manufactured and characterized for this complex, confirming the aforementioned complete resonant energy transfer from the ligands to the $Er^{3+}$ ion. The features of the reported device fabrication show a simple way to obtain large area NIR-OLEDs.

## Introduction

In recent years the research effort in luminescent lanthanide complexes with organic ligands has resulted in a great variety of materials for organic light-emitting diodes (OLEDs),[1] erbium doped fiber amplifiers (EDFAs)[2] and sensory technology.[3] The unique properties of lanthanide ions include narrow emission in the near infrared (NIR) range, large Stoke shifts and long luminescence lifetimes, and arise from their [Xe]4f$^n$ electronic configurations with many spectroscopic terms and energy levels. Erbium ion ($Er^{3+}$) is of particular interest due to its emission in the C-band (1.53–1.565 μm) of the silica optical telecommunication window.

Although f–f electronic transitions are forbidden by parity and spin rules, leading to very small absorption cross-sections and therefore low molar absorptivities, the lanthanide emission can be effectively sensitized *via* energy transfer from certain ligands used as "antennas" for ultraviolet-blue light.[4] The commonly accepted mechanism for such sensitization entails light absorption into the singlet state of the ligand, followed by population of the ligand triplet states *via* intersystem crossing (ISC), intramolecular energy transfer from the ligand triplet states to the emissive state(s) of the lanthanide, and finally characteristic light emission from the lanthanide.[5]

Efficient ligand to lanthanide energy transfer requires a good overlap between the triplet level phosphorescence of the ligand and the ground state absorption of some energy levels of the considered lanthanide. The most favourable ligands for complexes with $Eu^{3+}$ – and to a lesser extent with $Tb^{3+}$ and $Tm^{3+}$ – have been widely studied in connection with their visible emissions; however, the optimum ligands for lanthanides with infrared emissions are less studied.[6] In particular, 1.5 μm emission of $Er^{3+}$ has been reported for different molecular systems (including macrocyclic ligands, acyclic ligands and heterometallic functional assemblies)[7] but it is still required to explore new $Er^{3+}$ complexes to optimize their NIR emissivity.

β-Diketonates are amongst the sensitising ligands used.[8] Nevertheless, in contrast to their technological interest, the number of reliable NIR devices demonstrated is negligible. This is due to the fact that such organic ligands contain O–H and

C–H oscillators that, coordinated with the lanthanide ion, increase the non-radiative rates particularly for lanthanide states with low energy gap to the immediately lower state.

To overcome this situation, deuteration (C–D) and halogenation (C–F) of the organic ligands have proven to be successful approaches:[9] absorptions are diminished (C–D) or absent (C–F) because the third overtone of C–D is located at 1.5 μm and the third overtone of C–F is located at 2.6 μm. Halogenation is preferred for the C-band window because the third overtone of the C–D vibration absorbs in it. In addition, it should be noted that fluorination does not modify significantly the energy of the triplet levels, so the resonant transfer to the lanthanide ion is not affected.[10] In the late 1990s, Hasegawa *et al.* described the improved NIR luminescence of several deuterated and fluorinated $Ln^{3+}$ β-diketonate complexes in solution.[11]

To complete the coordination sphere of $Ln^{3+}$, oxygen-donor or nitrogen-donor Lewis bases are used, such as the *N*,*N*-donor ligands 1,10-phenanthroline (phen) and 2,2′-bipyridine (bipy). The resulting lanthanide complexes often show an intense luminescence attributed to the intramolecular energy transfer from the β-diketonate ligand to the *N*,*N*-donor.[12]

These *N*,*N*-donor ligands can be modified by substituents on the heterocycle rings. A rigid structure should be preferable since Yang *et al.*[13] reported a higher intensity of the sensitized luminescence for this type of antenna. An example of such a structure is bathophenanthroline (bath), used later with dibenzoylmethane by Kawamura *et al.*[14] who fabricated an evaporated OLED device with tris(dibenzoylmethane) mono-(bathophenanthroline)erbium(III) back in 2004, with an EL efficiency of $1 \times 10^{-5}$ lm $W^{-1}$.‡

In this work we have combined the two aforementioned improvements by adding fluorinated sensitising ligands and rigid and bulky antennas to the erbium trivalent ion, and designed a novel family of erbium complexes featuring 1,1,1-trifluoro-5,5-dimethyl-2,4-hexanedione (Htpm) as the fluorinated β-diketonate ligand and 2,2′-bipyridine (bipy), bathophenanthroline (bath) or 5-nitro-1,10-phenanthroline ($5NO_2$phen) as *N*,*N*-donor molecules, as part of a wider family of materials intended for use in the development of large area optoelectronic applications.[15]

Our work aims to point out how experimental data based on well documented synthetic strategies and characterization, including structural data, are of crucial importance for the interpretation of the photophysical properties to achieve the strongly demanded detailed understanding of the structure–property relationship,[16] which is required to provide guidelines to design lanthanide complexes with improved luminescence efficiency.

The synthesis, structure, DSC curves, FTIR and Raman studies of the new materials are reported. Besides, the visible photophysics and emission properties at 1.5 μm by exciting at different energies, together with their lifetimes, are investigated. Finally, we integrate the most promising complex, [Er(tpm)$_3$($5NO_2$phen)], into a full solution processed OLED with structure glass/indium-tin oxide (ITO)/poly(3,4-ethylenedioxythiophene)–poly(styrenesulfonate) (PEDOT:PSS)/active layer/Ca/Al, and the *J*–*V* and electro-luminescence responses are presented.

## Results and discussion

### Structural description

[Er(tpm)$_3$(bipy)] crystallizes in a triclinic centrosymmetric cell with two complexes per unit cell (Fig. 1, Table 1). Within each complex, the lanthanide ion is coordinated in a distorted square anti-prismatic fashion by six O atoms and two N atoms from the fluorinated β-diketonates and the ancillary ligand 2,2′-bipyridine, respectively. The Er–N distances are 2.515(4) and 2.542(4) Å and the Er–O distances are in the range of 2.282(4)–2.327(4) Å. The N–Er–N bite angle is 63°. The lanthanide ion is 1.41 and 1.16 Å out of the planes of the top (containing N atoms) and of the bottom square faces. The angle between the least-squares plane of such faces is just 3°. Molecules pack in dimers joined by π–π interactions with a distance between centroids of 3.811(4) Å and a slippage of 1.577 Å. This packing causes solvent accessible voids in the structure with a volume of 44 Å$^3$.

The mononuclear complexes in [Er(tpm)$_3$(bath)] crystallize in a monoclinic unit cell with the $P2_1/a$ space group (Fig. 2, Table 1). For each Er(III), the coordination environment includes six O atoms from the fluorinated sensitizing ligands and two N atoms from the bathophenanthroline neutral antenna, in a distorted square-antiprismatic geometry (Table 2). The bite angle N–Er–N is 64° and the N–Er distances are 2.512(5) and 2.524(5) Å. The trivalent ion sits approximately in the middle of the prism at a distance of 1.38/1.20 Å to the antiprismatic-square faces. Such faces are nearly parallel, making an angle of

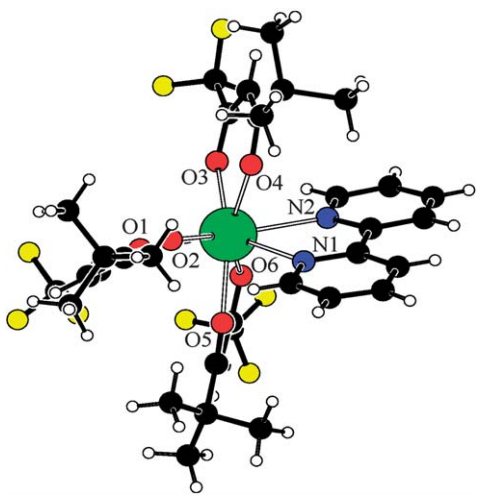


**Fig. 1** Structural diagram of [Er(tpm)$_3$(bipy)].

**Table 1** Crystal data and structure refinement

| Complex | [Er(tpm)$_3$(bipy)] | [Er(tpm)$_3$(bath)] | [Er(tpm)$_3$(5NO$_2$phen)] |
|---|---|---|---|
| Empirical formula | $C_{34}H_{38}ErF_9N_2O_6$ | $C_{48}H_{46}ErF_9N_2O_6$ | $C_{36}H_{37}ErF_9N_3O_8$ |
| Formula weight | 908.92 | 1085.13 | 977.95 |
| Temperature | 293(3) K | 293(3) K | 293(3) K |
| Wavelength | 0.71073 Å | 0.71073 Å | 0.71073 Å |
| Crystal system | Triclinic | Monoclinic | Monoclinic |
| Space group | *P*-1 | $P2_1/a$ | $P2_1/n$ |
| *a* | 9.6862(5) Å | 16.4630(5) Å | 14.2828(4) Å |
| *b* | 12.0313(6) Å | 14.2801(4) Å | 16.9860(5) Å |
| *c* | 18.1634(10) Å | 21.6052(7) Å | 18.2384(5) Å |
| $\alpha$ | 100.086(3)° | 90° | 90° |
| $\beta$ | 103.810(3)° | 99.901(2)° | 109.5580(11)° |
| $\gamma$ | 101.682(3)° | 90° | 90° |
| Volume | 1956.59(18) Å$^3$ | 5003.6(3) Å$^3$ | 4169.5(2) Å$^3$ |
| *Z* | 2 | 4 | 4 |
| Density (calculated) | 1.543 g cm$^{-3}$ | 1.440 g cm$^{-3}$ | 1.558 g cm$^{-3}$ |
| Erbium density | $0.978 \times 10^{21}$ cm$^{-3}$ | $1.250 \times 10^{21}$ cm$^{-3}$ | $1.042 \times 10^{21}$ cm$^{-3}$ |
| Absorption coefficient | 2.230 mm$^{-1}$ | 1.757 mm$^{-1}$ | 2.103 mm$^{-1}$ |
| *F*(000) | 906 | 2180 | 1948 |
| Crystal size | 0.25 × 0.12 × 0.10 mm$^3$ | 0.15 × 0.10 × 0.08 mm$^3$ | 0.15 × 0.07 × 0.07 mm$^3$ |
| $\theta$ range for data collection | 1.78–25.94° | 1.72–25.83° | 1.58–25.78° |
| Index ranges | $-11 < h < 11$;<br>$-14 < k < 14$;<br>$-22 < l < 22$ | $-20 < h < 20$;<br>$-17 < k < 17$;<br>$-26 < l < 26$ | $-17 < h < 17$;<br>$-20 < k < 20$;<br>$-22 < l < 22$ |
| Reflections collected | 19 836 | 40 965 | 40 051 |
| Independent reflections | 7513 | 9488 | 7975 |
| Completeness to $2\theta = 51°$ | 99.6% | 98.2% | 99.9% |
| Refinement method | Full matrix LS on $F^2$ | Full matrix LS on $F^2$ | Full matrix LS in $F^2$ |
| Data/restrains/parameters | 5907/0/477 | 4816/0/604 | 5008/6/503 |
| Goodness-of-fit on $F^2$ | 1.024 | 0.943 | 1.012 |
| Final *R* indices [$I > 2\sigma(I)$] | $R = 0.0442$; w$R = 0.1061$ | $R = 0.0519$; w$R = 0.0969$ | $R = 0.0436$; w$R = 0.0959$ |
| *R* indices (all data) | $R = 0.0640$; w$R = 0.1203$ | $R = 0.1331$; w$R = 0.1248$ | $R = 0.0865$; w$R = 0.1122$ |
| Largest diff. peak and hole | −1.649/1.526 | −0.552/0.650 | −0.409/0.661 |

less than 3°. The substituent phenyl rings do not share the central aromatic plane of phenanthroline, as seen by the torsion angles C2–C3–C19–C24 [64.7°] and C7–C10–C13–C18 [47.8°]. This rotation allows some C–H···centroid intermolecular contacts such as C18–H18···Cg5$^i$ (Cg5 is the centroid of the ring C19–C24 and *i*: $-½ + x$, $½ - y$, $z$). Solvent accessible voids with 71 Å$^3$ of volume exist in the crystal structure.

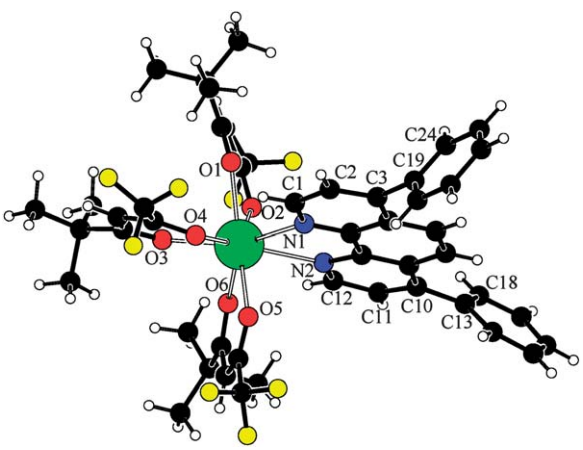


**Fig. 2** Structural diagram of [Er(tpm)$_3$(bath)].

[Er(tpm)$_3$(5NO$_2$phen)] crystallizes in the monoclinic space group $P2_1/n$ with four complexes in the unit cell (Fig. 3, Table 1). In each complex, the $Er^{3+}$ ion is eight times coordinated with six oxygen atoms from the fluorinated β-diketonates and two nitrogen atoms from the 5-nitro-1,10-phenanthroline moiety forming a distorted square-antiprismatic prism. There are signs of disorder in the structure: the terminal fluoro and methyl groups exhibit large displacement factors and two positions could be found for the 5-nitro-1,10-phenanthroline with occupation of roughly 50%. The erbium ion occupies the centre of the prism with a distance 1.38 Å to the square face containing

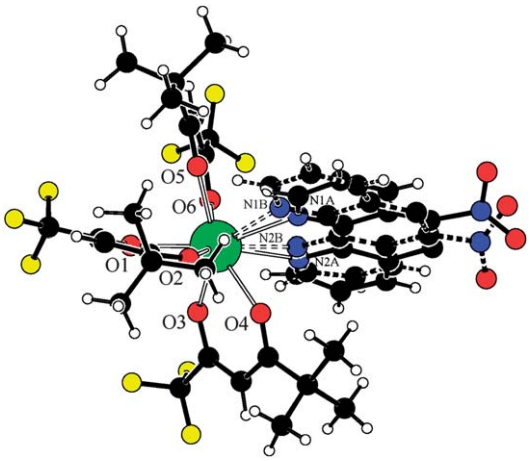


**Fig. 3** Structural diagram of [Er(tpm)$_3$(5NO$_2$phen)], a few hydrogen atoms were omitted for clarity.

the N atoms and 1.18 Å to the opposite face. The bite angle is 62/67° for N1A–Er–N2A and for N1B–Er–N2B, respectively. The Er–X distances range from 2.266(4) to 2.322(4) Å for the O atoms and 2.415(13) to 2.452(16) for the N atoms (Table 2). There are no classic hydrogen bonds between the complexes due to the lack of donors; only some weak C–H···X intermolecular contacts can be discerned. The complexes pack very efficiently in the crystal leaving no solvent accessible voids.

### X-ray powder diffraction

Fig. 4 shows the experimental diffraction pattern of the three $Er^{3+}$ complexes. In the same figure simulated powder patterns from the single crystal structure using PLATON[17] can be seen. There is an excellent match between simulated and experimental diffractograms; the peaks appear at the predicted theta angles at the same relative intensities. The experimental diffractograms show a background higher for low theta angles as expected from the diffuse scattering of X-rays by glass and air, a common characteristic when using rotating capillaries in the Debye–Scherrer geometry. Powder diffraction shows that all the material synthesized contains the same structure as the small single crystals used for single-crystal X-ray diffraction.

### Differential scanning calorimetry

The DSC curves of these complexes (Fig. 5) show two main thermal effects: one between 134 and 208 °C (melting point) and another at around 330 °C (decomposition point). The decomposition temperatures indicate that the studied complexes have good thermal stability and are in agreement with the conclusion reported that a fluorinated substituent in the ligands leads to improved thermal and oxidative stability and increases the volatility of the complex.[18,19] The improved thermal stability and volatility result in good film-forming ability which facilitates the fabrication of electroluminescent devices.

### Infrared spectra

IR spectra (not shown for the sake of brevity) of the complexes in the region of 900–575 cm$^{-1}$ exhibit the absorption bands characteristic for *N*,*N*-donor molecules: 645, 740 and 764 cm$^{-1}$ for the complex containing 2,2′-bipyridine; 574, 630, 702, 746, 766 and 795 cm$^{-1}$ for the complex containing bathophenanthroline ancillary ligand and 737, 749 and 836 cm$^{-1}$ for the complex with 5-nitro-1,10-phenanthroline. The band at 746 cm$^{-1}$ and that at 1017 cm$^{-1}$ are attributed to ring breathing

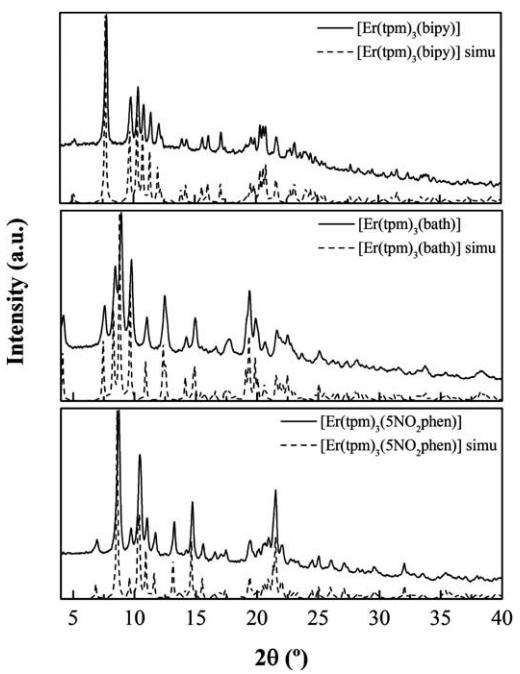


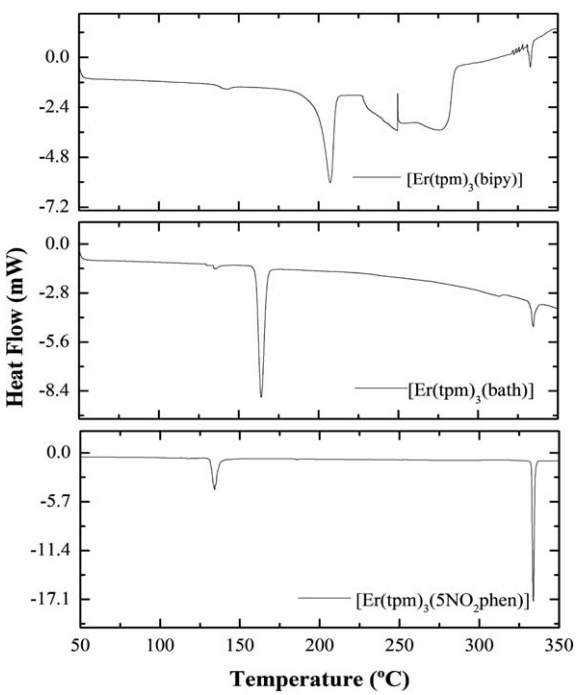


**Fig. 4** Comparison between experimental and simulated diffraction patterns.

modes. The bands assigned to ring stretching modes CN, $CC_{str}$ ($B_1$ symmetry) can be observed in the range of 1600–1500 $cm^{-1}$. They are shifted in comparison with those of the free ligand, which indicates that the *N*,*N*-donor molecules are coordinated to erbium(III).[20]

Bands at around 850 $cm^{-1}$ come from the β-diketonate ligand and are attributed to C–H twisting bending vibrations. They are appreciably red shifted in comparison with those in free ligands due to the perturbation induced by coordination to the metal ion.[21]

Further good evidence for the complexation in the studied $Er^{3+}$ complexes is obtained by the observation of C=O stretching bands around 1600 $cm^{-1}$, shifted *vs.* those of the free ligands.[22] In addition, the broad bands observed in free β-diketonate ligands become narrower in the complexes.[23]

An important feature common to all fluorinated complexes is the occurrence of strong absorption bands from 1139 to 1115 $cm^{-1}$, assigned to $CF_3$ as (C–F) stretching modes.

### Raman spectra

Raman spectra of the complexes show peaks at 1600, 1302, 1065, 700, 465 and 170 $cm^{-1}$ for the complex containing 2,2′-bipyridine; at 1605, 1455, 1301, 700 and 428 $cm^{-1}$ for the complex containing bathophenanthroline; and at 1608, 1456, 1346, 1053, 711, 416 and 89 $cm^{-1}$ for the complex with 5-nitro-1,10-phenanthroline. It is known that the introduction of additional neutral ligands such as bipy, bath or $5NO_2$phen into the inner sphere weakens the Er–O (Htpm) bonds to facilitate the coordination to the *N*,*N*-donor molecule (Er–N), resulting in very stable octacoordinated complexes, in agreement with the X-ray structural data and the results from FTIR spectroscopy.

### Optical absorption

**Absorption spectra.** Fig. 6a shows the absorption spectra for the Er-complexes in $10^{-5}$ M methanol diluted solutions. Er ion transitions are not observed, since the f–f transitions are too weak to be detected at this concentration. The absorption bands are associated with the organic ligand π–π* transitions with maxima at 283, 279 and 290 nm for [Er(tpm)$_3$(bipy)], [Er(tpm)$_3$(bath)] and [Er(tpm)$_3$($5NO_2$phen)], respectively. The optical energy gaps ($E_g$) of the complexes (departure from zero in the second derivatives of the absorption spectra, not shown) are: 3.57, 3.53 and 3.09 eV, respectively. The broadest absorption band corresponds to [Er(tpm)$_3$($5NO_2$phen)], which has the most efficiently packed structure, as discussed in the structural description section.

Increasing the solution concentration up to $10^{-3}$ M (Fig. 6b) allows us to observe the sharp f–f transitions from the $^4I_{15/2}$ ground state of the $Er^{3+}$ ion overlapped with the organic ligands absorption. The strongest transitions correspond to $^4G_{11/2}$ (378 nm) and to the structured $^2H_{11/2}$ (519 nm) plus $^4S_{3/2}$ (543 nm) absorptions. It is also possible to observe the transitions associated with $^2H_{9/2}$ (407 nm), $^4F_{5/2}$ (451 nm), $^4F_{7/2}$ (488 nm) and $^4F_{9/2}$ (655 nm) levels.[24]

The intensity of $^4I_{15/2} \rightarrow {}^2H_{11/2}$, $^4S_{3/2}$ hypersensitive transitions depends on the site symmetry and anisotropy.[25] The three different environments of $Er^{3+}$ considered here have the same $C_1$ symmetry, but the anisotropy of the compound with the $5NO_2$phen ancillary ligand in the first coordination sphere is significantly lower than in the bipy and bath cases (see bond distances in Table 2). Correspondingly, the intensity of this transition in [Er(tpm)$_3$($5NO_2$phen)] is larger than in the other two.

Fig. 6c shows several band sets corresponding either to f–f Er transitions or to C–H vibrations. $^4I_{15/2} \rightarrow {}^4I_{11/2,13/2}$ bands appear at around 980 nm and 1500–1600 nm, respectively. In both cases, some band structure associated with the Stark's components for the ground $^4I_{15/2}$ multiplet is observed.

Fig. 6c also shows the second and third overtones of the aromatic C–H stretching vibration, which appear near 1675 nm and 1140 nm, respectively.

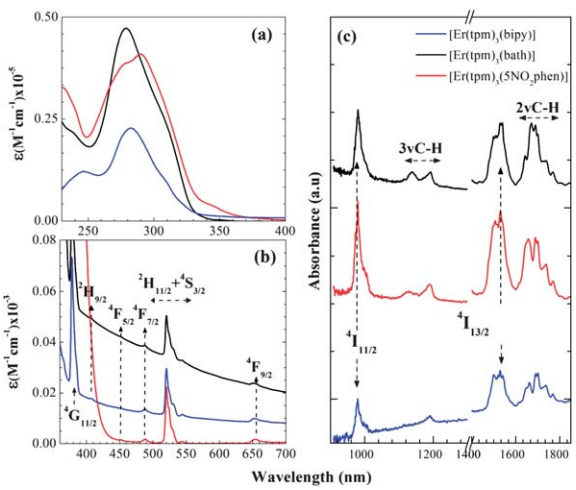


### Luminescence

**Visible photoluminescence emission.** The emission of the novel $Er^{3+}$ complexes in the visible region (300–700 nm), associated with the organic part of the complexes, has been studied under direct excitation of the ligands at $\lambda = 270$ nm. Fig. 7a shows the PL emission of the three complexes in $10^{-3}$ M methanol solutions, so that their intensities can be directly compared to each other. The [Er(tpm)$_3$(bath)] complex exhibits the most intense one, with a maximum at 382 nm and a first vibronic band at 398 nm. That from [Er(tpm)$_3$(bipy)] is significantly weaker (×0.04 factor), but well resolved emission peaking at 404 nm, with vibronic shoulders corresponding to 1302 and 1600 $cm^{-1}$ phonons, can still be observed. However, for the [Er(tpm)$_3$($5NO_2$phen)] complex the emission from the organic ligands is completely quenched.

We have measured the relative efficiency PL quantum yield (PLQY), $\Phi$, as explained in the Experimental section, by comparing to perylene in $10^{-6}$ M methanol solutions ($\Phi = 0.92$).[26] The measured PLQY is $1.12 \times 10^{-2}$ for [Er(tpm)$_3$(bath)]. At this concentration no emission could be detected from the other two complexes.

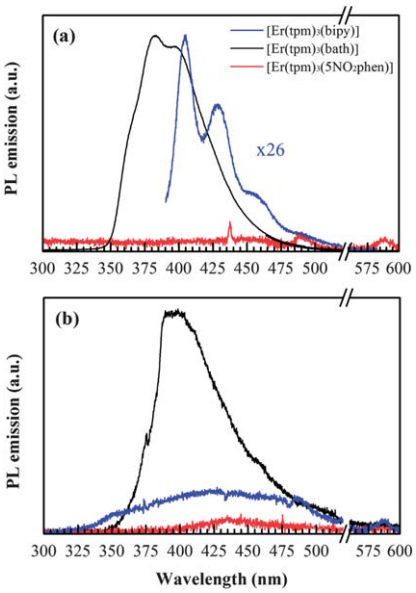


**Fig. 7** PL emission measured under 270 nm excitation wavelength for (a) methanol solutions and (b) powder. A break has been inserted where the laser harmonic is $\lambda = 540$ nm for the sake of clarity.

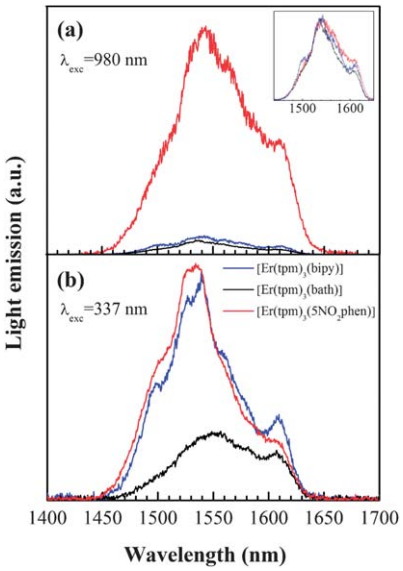


**Fig. 8** Infrared $^4I_{13/2} \rightarrow {}^4I_{15/2}$ emission spectra under excitation of: (a) the Er $^4I_{11/2}$ level (980 nm) and (b) the organic ligands with 337 nm excitation wavelength. The inset shows the normalized emissions.

The emission spectrum in powder (Fig. 7b) shows a less resolved structure, slightly shifted to the red region in comparison to that in solution (maximum at 395 nm) as a result of the aggregation state. Even though the intensities of the spectra in powder form cannot be strictly compared, assuming the same incident energy density, we can qualitatively observe the same behaviour as in solution.

It should be noted that the emission from the organic part of the $[Er(tpm)_3(5NO_2phen)]$ complex – which was totally quenched in solution – is also negligible in powder. The quenching of the visible emission of the complexes is related to the efficiency of the energy transfer capability from the ligand to the $Er^{3+}$ ion, the so-called *antenna effect*. At the same time, it is to be expected that the characteristic NIR emission of the Er: $^4I_{13/2} \rightarrow {}^4I_{15/2}$ transition is favoured (as it is shown in the next section).

**Infrared photoluminescence emission.** Fig. 8a shows a qualitative comparison between the $Er^{3+}$: $^4I_{13/2} \rightarrow {}^4I_{15/2}$ emission intensities at room temperature for the three complexes excited at 980 nm ($^4I_{11/2}$ level), provided that all the samples were measured under the same conditions. It is noticeable that $[Er(tpm)_3(5NO_2phen)]$ complex emission is much higher, in agreement with the structural findings: the absence of solvent-accessible voids and shorter Er–N distances. This higher emission in the NIR, together with the quenching of the organic ligand emission (mentioned above), is indicative of a good energy transfer from the organic ligand to the $Er^{3+}$ ion in the resulting environment of the $[Er(tpm)_3(5NO_2phen)]$ complex. The normalized spectra are shown in the inset of Fig. 8a: the band structure shows maxima at 1543 nm in all cases, with additional weaker bands surrounding. This structure is mainly due to the Stark level distribution of the fundamental multiplet $^4I_{15/2}$.

The PL decay of the $^4I_{13/2}$ multiplet was measured after $^4I_{11/2}$ excitation (Fig. 9). The light intensity ($I$) decay with time ($t$) has been analysed by a single exponential law, $I(t) = I(t = 0) \times \exp(-t/\tau)$, where $\tau$ is the lifetime of the level. Despite the possible PL reabsorption, the decays obtained after 980 nm excitation show a single exponential behaviour, which can be observed as a line in the semi-log representations of Fig. 9. The $^4I_{13/2}$ lifetimes obtained for the three complexes, namely $\tau =$ 1.77, 1.55 and 1.53 μs for $[Er(tpm)_3(bipy)]$, $[Er(tpm)_3(bath)]$ and $[Er(tpm)_3(5NO_2phen)]$, respectively, are similar between them and to other Er complexes previously reported.[27] Taking into account that the radiative lifetime ($\tau_{rad}$) of $Er^{3+}$ ranges $\tau =$ 2–3 ms, the quantum efficiency ($\eta$) of these compounds is $\eta = \tau/\tau_{rad} \approx 0.1\%$.

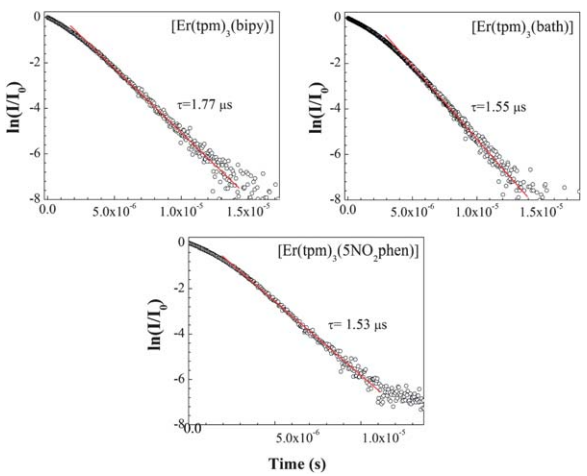

So as to further investigate the energy transfer from the organic ligand to the $Er^{3+}$ ion, the emission at 1.5 μm ($Er^{3+}$: $^4I_{13/2} \rightarrow {}^4I_{15/2}$ transition) was measured, by exciting the organic ligand at $\lambda_{exc} = 337$ nm ($N_2$ laser). In Fig. 8b the emission spectra are presented for the three complexes, measured under the same conditions. $[Er(tpm)_3(5NO_2phen)]$ and $[Er(tpm)_3(bipy)]$ complexes show similar intensities, higher than that of $[Er(tpm)_3(bath)]$. The structures of these bands are quite similar to those obtained by exciting directly the $Er^{3+}$ levels at $\lambda_{exc} = 980$ nm (inset in Fig. 8a).

We confirm again the behaviour observed for visible emission: an inverse relationship between the intensity of $Er^{3+}$: $^4I_{13/2} \rightarrow {}^4I_{15/2}$ emission and visible emission of the organic ligand.

**Electroluminescence (EL) emission.** In order to check if the observed antenna effect also takes place when the emission is excited with an applied voltage and taking advantage of the good film forming properties, a full solution processed simple structure OLED based on the $[Er(tpm)_3(5NO_2phen)]$ complex, manufactured as described in the Experimental part, was fabricated. Fig. 10 shows the *J–V* response measured from ITO/PEDOT:PSS (70 nm)/active layer (170 nm)/Ca/Al. The diode exhibits a good electrical performance, with a threshold voltage of a few volts (7 V), similar to that reported by Wei *et al.*[28] for a multilayer vacuum-deposited device and further lower than that reported for the ErQ-based device.[29] Moreover, the very low noise level is indicative of the quality of the layer.

In the same figure, we can observe $Er^{3+}$: $^4I_{13/2} \rightarrow {}^4I_{15/2}$ EL emission, measured at 2 mA driving current, with maximum at 1535 nm, together with the PL emissions obtained by exciting $Er^{3+}$ at 980 nm and the organic ligands at 337 nm.

The EL spectrum matches very well with the photoluminescence spectra, except for a narrowing at the low energy wing of the band. This effect is most likely related to an increase in the temperature of the material and consequently to the redistribution of the electronic population in the excited $^4I_{13/2}$ multiplet. Furthermore, as again no ligand electroluminescence emission is observed, the charge carrier transfer process that takes place and which results in the $Er^{3+}$ 1.5 μm emission has to be very similar to that of the PL indirect excitation explained above.

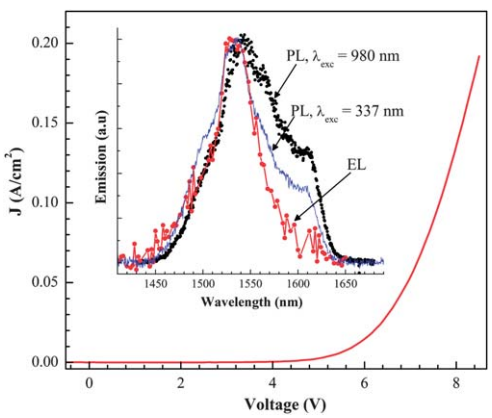


## Conclusions

Three novel $Er^{3+}$ complexes with fluorinated β-diketonate and *N*,*N*-donor molecules as ligands have been synthesized and their structures have been determined by single-crystal X-ray diffraction. The differences in Er–N and Er–O bond distances have been rationalized in terms of the electronic and steric properties of the ligands.

Through a thorough characterization of the photophysical properties of the $Er^{3+}$ complexes, we have been able to confirm the influence of utilizing certain ligands as "antenna": this choice determines the efficiency of the packing in the crystal and the presence of solvent-accessible voids, the length of the Er–N distances and the effectiveness of the resonant energy transfer.

Out of the three new complexes, $[Er(tpm)_3(5NO_2phen)]$ has the best structural features: it shows a compact structure which prevents the deleterious effects of solvent molecules, has shorter Er–N distances and a complete energy transfer by the *antenna effect* has been achieved. These characteristics, together with its good processability and thin film forming properties, have allowed its integration into a full solution processed OLED, paving the way to obtain large area NIR-OLEDs. This device, when excited with an applied voltage, shows a total quenching of the visible emission and a 1.54 μm EL response very similar to the photoluminescence spectrum, thus confirming the activation *via* efficient energy-transfer from the ligand to the $Er^{3+}$ ion.

## Experimental

### Materials

All reagents and solvents employed were commercially available and used as supplied without further purification. All the procedures for complex preparation were carried out under nitrogen and using dry reagents to avoid the presence of water and oxygen, which can quench metal photoluminescence.

### Synthesis

The complex $[Er(tpm)_3(bipy)]$ was obtained as follows: under stirring, 1,1,1-trifluoro-5,5-dimethyl-2,4-hexanedione (3 mmol) methanol solution (20 ml) is added to a 1 mmol of $Er(NO_3)_3 \cdot 5H_2O$ in methanol. The mixture is neutralized by adding potassium methoxide (3 mmol) dropwise under vigorous stirring until potassium nitrate precipitates. $KNO_3$ is removed by decanting, and 2,2′-bipyridine (1 mmol) is finally added. The mixture is heated to 75 °C and stirred overnight, then washed with dioxane, and finally dried in vacuum to give the product in 90–95% yield (based in Er). Crystals suitable for X-ray analysis were obtained by slow evaporation of a methanol–dioxane solution at RT. The synthesis procedure for $[Er(tpm)_3(bath)]$ and $[Er(tpm)_3(5NO_2phen)]$ is analogous, using

1 mmol of bathophenanthroline or 5-nitro-1,10-phenanthroline, respectively, instead of 2,2′-bipyridine.

[Er(tpm)$_3$(bipy)]: chemical formula: $C_{34}H_{38}ErF_9N_2O_6$. $M_w$: 908.92. Anal. calcd for $C_{34}H_{38}ErF_9N_2O_6$: C, 44.88; H, 4.18; Er, 18.40; F, 18.80; N, 3.08; O, 10.56. Found: C, 44.81; H, 4.26; N, 2.98%.

[Er(tpm)$_3$(bath)]: chemical formula: $C_{48}H_{46}ErF_9N_2O_6$. $M_w$: 1085.13. Anal. calcd for $C_{48}H_{46}ErF_9N_2O_6$: C, 53.08; H, 4.24; Er, 15.41; F, 15.75; N, 2.65; O, 8.85. Found: C, 52.91; H, 4.30; N, 2.58%.

[Er(tpm)$_3$(5NO$_2$phen)]: chemical formula: $C_{36}H_{37}ErF_9N_3O_8$. $M_w$: 976.94. Anal. calcd for $C_{36}H_{37}ErF_9N_3O_8$: C, 44.22; H, 3.78; Er, 17.12; F, 17.49; N, 4.29; O, 13.11. Found: C, 44.09; H, 3.86; N, 4.18%.

### X-ray crystallographic analysis

For the determination of crystal structures by X-ray diffraction, crystals of [Er(tpm)$_3$(bipy)], [Er(tpm)$_3$(bath)] and [Er(tpm)$_3$(5-NO$_2$phen)] were glued in glass fibers and mounted on an BruKer APEX II diffractometer. Diffraction data were collected at room temperature 293(2) K using graphite monochromated Mo K$\alpha$ ($\lambda$ = 0.71073 Å) radiation. Absorption corrections were made using SADABS.[30] The structures were solved by direct methods using SHELXS-97 (ref. 31) and refined anisotropically (non-H atoms) by full-matrix least-squares on $F^2$ using the SHELXL-97 program.[31] PLATON[17] was used to analyse the structure and figure plotting. Atomic coordinates, thermal parameters and bond lengths and angles have been deposited at the Cambridge Crystallographic Data Centre (CCDC).

### Physical measurements

The C, H, N elemental analyses were made for all $Er^{3+}$ complexes using a Perkin Elmer CHN 2400 apparatus.

Differential scanning calorimetry (DSC) data were obtained on a DSC TA instrument mod Q100 v.9.0 with a heating rate of 10 °C min$^{-1}$ under a $N_2$ atmosphere.

Infrared spectra of Er complexes were recorded using a Thermo Nicolet 380 FT-IR apparatus in KBr pellets.

The Raman spectra were recorded using a FT-Raman Bruker FRA106 by using a Nd:YAG laser, 1064.1 nm, to excite the sample.

Powder diffractograms of erbium complexes were obtained using an ENRAF-NONIUS FR590 powder diffractometer with an INEL120 detector (Debye–Scherrer geometry).

### Optical measurements

Optical absorption and photoluminescence spectra of the materials in solution or powder were measured at room temperature. The 200–800 nm range absorption spectra were recorded with a Cary 4000 Varian spectrophotometer. The absorbance in the 900–3500 nm NIR range was recorded using a Varian 660-IR FT-IR spectrometer in KBr pellets. Visible PL spectra were excited with the 270 nm line of an OPO laser (NT-342A-SH, EKSPLA) and collected using a Jobin-Yvon HR 460 monochromator coupled to an intensified CCD digital camera (4Picos, Stanford Computer Optics). All the emission spectra have been corrected by the spectral response of the experimental setups.

The PLQY of the complexes, $\Phi$, was measured in $10^{-6}$ M methanol optically diluted solutions (OD < 0.1 at the excitation wavelength, $\lambda_{exc}$ = 270 nm), taking perylene as a reference emitter ($\Phi_r$ = 0.92).[26] The quantum yield was calculated from the following equation:

$$\phi_x = \frac{A_r}{A_x}\frac{E_x}{E_r}\frac{n_x}{n_r}\phi_r \quad (1)$$

where $A$ is the absorbance at the excitation wavenumber, $E$ is the area under the corrected (by spectral response of the experimental setups) emission curve (expressed in number of photons), and $n$ is the refractive index of the solvents used. The subscripts r and x denote the reference and the unknown, respectively.

The NIR PL emission at 1.5 μm was excited both at the ligand absorption, $\lambda_{exc}$ = 337 nm, and at $Er^{3+}$:$^4I_{11/2}$ transition, $\lambda_{exc}$ = 980 nm, with a $N_2$ laser and a MOPO laser system, respectively. The emitted light was dispersed using a SPEX (model 340E, $f$ = 34 cm) spectrometer and detected with a Peltier-cooled NIR Hamamatsu photomultiplier and a lock-in amplifier. Lifetimes were measured by using a Tektronix (model TDS 520, 500 MHz) oscilloscope. NIR EL spectra from diodes were analysed using a SPEX 1702/04 ($f$ = 1 m) monochromator and detected with a 77 K cooled Ge detector connected to a Stanford Research system SR530 locking amplifier, using 50% duty cycle waveform from a TTi40 MHz arbitrary waveform generator and a TREK-601C amplifier.

### Device fabrication and evaluation

The structure of the devices is ITO/PEDOT:PSS/active layer/cathode. Pre-patterned ITO glass plates with four circular diodes (1 mm and 1.5 mm radii) were extensively cleaned, using chemical and UV-ozone methods, just before the deposition of the organic layers. PEDOT:PSS (CLEVIOS P VP AI 4083) was deposited at 2000 rpm by spin-coating and then cured on a hot plate at 120 °C for 15 min. The active layers were deposited by spin coating (1500 rpm) and cured on a hot plate at 90 °C for 10 min plus 120 °C for 10 min in order to complete solvent removal. Precursor 4 wt% methanol solutions were kept in an ultrasonic bath for 45 min and filtered through a 0.2 μm polytetrafluoroethylene (PTFE) syringe filter, prior to being spin coated. The thickness of the layers was measured using an Alpha step 200 profilometer (Tenkor Instruments), obtaining 70 nm for the PEDOT:PSS layer and 170 nm for the active layer. The cathode was thermally evaporated in an atmosphere of $8 \times 10^{-6}$ Torr on top of the organic layer and finally the structure was encapsulated using a glass cover attached by a bead of epoxy adhesive [EPO-TEK(730)]. All the process was carried out in an inert atmosphere glovebox (<0.1 ppm $O_2$ and $H_2O$).

Current density–voltage ($J$–$V$) characteristics were measured using a semiconductor parameter analyser Agilent 4155C and a SMU pulse generator Agilent 41501B. A pulse train was used as an input signal. The duty cycle was set to be 0.2%, thus having a pulse width of 0.5 ms for a period of 100 ms. The refresh time

 

between two consecutive pulses ensures long time operation without significant device degradation. Furthermore, the *J–V* curve stability was achieved by gradually increasing the pulse amplitude up to the point where reproducible measurements were observed.

## Acknowledgements

P. Martín-Ramos would like to thank Fulbright Commission and the Spanish Ministry of Education for their financial support and Prof. P. Chamorro-Posada and Prof. L. M. Navas-Gracia for their insightful discussions. M. Ramos-Silva is grateful to the Fundação para a Ciência e a Tecnologia (FCT) for providing funds under grants PTDC/FIS/102284/2008 and PEst-C/FIS/UI0036/2011. Support by Comunidad Autónoma de Madrid under project S2009/MAT-1756 and by the Spanish Ministerio de Economía y Competitividad under projects MAT2009-08786, TEC2009-13991-C02-02 and TEC2011-13635-E is gratefully acknowledged by C. Coya. The authors would also like to thank the ISOM (UPM) for granting access to their technical facilities.

## Notes and references

1 J. Kido and Y. Okamoto, *Chem. Rev.*, 2002, **102**, 2357; H. You, J. Fang, Y. Xuan and D. Ma, *Mater. Sci. Eng., B*, 2006, **131**, 252; M. A. Katkova and M. N. Bochkarev, *Dalton Trans.*, 2010, **39**, 6599; A. de Bettencourt-Dias, *Dalton Trans.*, 2007, **22**, 2229; S. V. Eliseeva and J. C. G. Bunzli, *Chem. Soc. Rev.*, 2010, **39**, 189–227.

2 C. Chen, D. Zhang, T. Li, D. Zhang, L. Song and Z. Zhen, *J. Nanosci. Nanotechnol.*, 2010, **10**, 1947; C. Chen, D. Zhang, T. Li, D. Zhang, L. Song and Z. Zhen, *Appl. Phys. Lett.*, 2009, **94**, 041119.

3 J. G. Bunzli, *Acc. Chem. Res.*, 2006, **39**, 53; J. P. Leonard and T. Gunnlaugsson, *J. Fluoresc.*, 2005, **15**, 585.

4 S. I. Weissman, *J. Chem. Phys.*, 1942, **10**, 214; E. B. van der Tol, H. J. van Ramesdonk, J. W. Verhoeven, F. J. Steemers, E. G. Kerver, W. Verboom and D. N. Reinhoudt, *Chem.–Eur. J.*, 1998, **4**, 2315; A. P. Bassett, S. W. Magennis, P. B. Glover, D. J. Lewis, N. Spencer, S. Parsons, R. M. Williams, L. De Cola and Z. Pikramenou, *J. Am. Chem. Soc.*, 2004, **126**, 9413.

5 G. A. Crosby, R. E. Whan and J. J. Freeman, *J. Phys. Chem.*, 1962, **66**, 2493; R. E. Whan and G. A. Crosby, *J. Mol. Spectrosc.*, 1962, **8**, 315; F. J. Steemers, W. Verboom, D. N. Reinhoudt, E. B. van der Tol and J. W. Verhoeven, *J. Am. Chem. Soc.*, 1995, **117**, 9408.

6 E. Brunet, O. Juanes and J. C. Rodriguez-Ubis, *Curr. Chem. Biol.*, 2007, **1**, 11; L. Armelao, S. Quici, F. Barigelletti, G. Accorsi, G. Bottaro, M. Cavazzini and E. Tondello, *Coord. Chem. Rev.*, 2010, **254**, 487.

7 S. Comby and J. C. G. Bünzli, Lanthanide Near-Infrared Luminescence in Molecular Probes and Devices, in *Handbook on the Physics and Chemistry of Rare Earths*, ed. K. A. Gschneidner, J. C. G. Bünzli and V. K. Pecharsky, Elsevier, Amsterdam, 2007, vol. 37, ch. 235, p. 217.

8 K. Binnemans, Rare-earth beta-diketonates, in *Handbook on the Physics and Chemistry of Rare Earths*, ed. K. A. Gschneidner, J. C. G. Bünzli and V. K. Pecharsky, Elsevier, Amsterdam, 2005, vol. 35, ch. 225, p. 107; K. Binnenmans, *Chem. Rev.*, 2009, **109**, 4283.

9 A. P. Bassett, R. Van Deun, P. Nockemann, P. B. Glover, B. M. Kariuki, K. Van Hecke, L. VanMeervelt and Z. Pikramenou, *Inorg. Chem.*, 2005, **44**, 2754.

10 S. Pietrantoni, R. Francini, R. Pizzoferrato, S. Penna, R. Paolesse and F. Mandoj, *Phys. Status Solidi C*, 2007, **4**, 1048.

11 Y. Hasegawa, K. Murakoshi, Y. Wada, S. Yanagida, J. H. Kim, N. Nakashima and T. Yamanaka, *Chem. Phys. Lett.*, 1996, **248**, 8; Y. Hasegawa, K. Murakoshi, Y. Wada, J. H. Kim, N. Nakashima, T. Yamanaka and S. Yanagida, *Chem. Phys. Lett.*, 1996, **260**, 173; Y. Hasegawa, Y. Kimura, K. Murakoshi, Y. Wada, J. H. Kim, N. Nakashima, T. Yamanaka and S. Yanagida, *J. Phys. Chem.*, 1996, **100**, 10201; M. Iwamuro, Y. Hasegawa, Y. Wada, K. Murakoshi, T. Kitamura, N. Nakashima, T. Yamanaka and S. Yanagida, *Chem. Lett.*, 1997, 1067; Y. Hasegawa, M. Iwamuro, K. Murakoshi, Y. Wada, R. Arakawa, T. Yamanaka, N. Nakashima and S. Yanagida, *Bull. Chem. Soc. Jpn.*, 1998, **71**, 2573; M. Iwamuro, Y. Wada, T. Kitamura, N. Nakashima and S. Yanagida, *Phys. Chem. Chem. Phys.*, 2000, **2**, 2291; S. Yanagida, Y. Hasegawa and Y. Wada, *J. Lumin.*, 2000, **87–89**, 995; S. Yanagida, Y. Hasegawa, K. Murakoshi, Y. Wada, N. Nakashima and T. Yamanada, *Coord. Chem. Rev.*, 1998, **171**, 461.

12 Y. X. Zheng, J. L. Liang, Q. Lin, Y. N. Yu, Q. G. Meng, Y. H. Zhou, S. B. Wang, H. A. Wang and H. J. Zhang, *J. Mater. Chem.*, 2001, **11**, 2615.

13 X. D. Yang, Y. Y. Ci and W. B. Chang, *Anal. Chem.*, 1994, **66**, 2590; Y. S. Yang, M. L. Gong, Y. Y. Li, H. Y. Lei and S. L. Wu, *J. Alloys Compd.*, 1994, **207–208**, 112.

14 Y. Kawamura, Y. Wada and S. Yanagida, *Jpn. J. Appl. Phys.*, 2001, **40**, 350.

15 J. Martín-Gil, P. Martín-Ramos, P. Chamorro-Posada, L. M. Navas-Gracia, A. M. Matos-Beja, M. Ramos-Silva, A. L. Álvarez-Castillo and C. Coya-Párraga, *Optically active erbium(III) and ytterbium(III) octacoordinated ternary complexes and preparation methods*, International Patent Pub. no. WO2012120175, Application no.: PCT/ES2012/070143, 07/03/2012.

16 F. Artizzu, M. L. Mercuri, A. Serpe and P. Deplano, *Coord. Chem. Rev.*, 2011, **255**, 2514.

17 A. L. Spek, *J. Appl. Crystallogr.*, 2003, **36**, 7.

18 J. B. Yu, L. Zhou, H. J. Zhang, Y. X. Zheng, H. R. Li, R. P. Deng, Z. P. Peng and Z. F. Li, *Inorg. Chem.*, 2005, **44**, 1611.

19 Y. X. Zheng, L. S. Fu, Y. H. Zhou, J. B. Yu, Y. N. Yu, S. B. Wang and H. J. Zhang, *J. Mater. Chem.*, 2002, **12**, 919.

20 C. K. Pearce, D. W. Grosse and W. Hessel, *J. Chem. Eng. Data*, 1970, **15**, 567.

21 G. B. Deacon and R. I. Phillips, *Coord. Chem. Rev.*, 1980, **33**, 227.

22 K. Nakamoto, *Infrared and Raman spectra of inorganic and coordination compounds*, Wiley, 6th edn, 2009.

23 S. P. Vila Nova, H. J. Batista, S. Alves, C. de Mello Donegá, R. L. Longo, G. F. de Sa and L. C. Thompson, *J. Lumin.*, 2006, **118**(1), 83.
24 C. Görller-Walrand and K. Binnemans, Spectral intensities of f–f transitions, in *Handbook on the physics and chemistry of rare earths*, ed. K. A. Gschneidner and L. Eyring, Elsevier, Amsterdam, 1998, vol. 25, ch. 167, p. 101.
25 S. A. Davis and F. S. Richardson, *Inorg. Chem.*, 1984, **23**, 184.
26 M. Montalti, A. Credi, L. Prodi and M. T. Gandolfini, *Handbook of Photochemistry*, CRC Press LLC, Boca Raton, FL, 3rd edn, 2005.
27 Z. Li, J. Yu, L. Zhou, H. Zhang, R. Deng and Z. Guo, *Org. Electron.*, 2008, **9**, 487; X. Li, Z. Si, C. Pan, L. Zhou, Z. Li, X. Li, J. Tang and H. Zhang, *Inorg. Chem. Commun.*, 2009, **12**, 675.
28 F. Wei, Y. Z. Li, G. Z. Ran and G. G. Qin, *Opt. Express*, 2010, **18**, 13542.
29 R. J. Curry, W. P. Gillin, A. P. Knights and R. Gwilliam, *Appl. Phys. Lett.*, 2000, **77**(15), 2271.
30 G. M. Sheldrick, *SADABS*, University of Göttingen, Germany, 1996.
31 G. M. Sheldrick, *SHELXL97 and SHELXS97*, University of Göttingen, Germany, 1997.
32 Z. Li, J. Yu, L. Zhou, H. Zhang, R. Deng and Z. Guo, *Org. Electron.*, 2008, **9**, 487.

 